Journal of Computational Applied Mechanics 2024, 55(-): PP-PP

DOI: 10.22059/JCAMECH.2024.371356.945

RESEARCH PAPER

Elastostatic behaviour of functionally graded porous beam: novel Kuhn Tucker conditions with R program for mathematical computing

Geetha Narayanan Kannaiyan [a, b, *], Balasubramaniam Vivekanandam [a]

[a] *Faculty of computer science and multimedia, Lincoln University College, Malaysia*
[b] *Department of Mathematics, Dayananda sagar college of engineering, Bengaluru 560078, India*

Abstract

Pores affect functionally graded materials. Further characteristics may be added if pores expand from the surface to the interior. Functionally graded porous beam (FGPB) bending response is analyzed using a specific shear shape function that accounts for both uniform and uneven porosity distributions. Power law changes the material characteristics of FGPBs with uniform and uneven porosity distributions along length and thickness. In order to determine the maximum transverse deflections, axial stresses, transverse shear stresses, and normal stresses in simply-supported and clamped-clamped beams, numerical calculations are performed with various gradation exponents, aspect ratios (L/h), and porosity levels (both even and uneven). The obtained results are compared with earlier investigations and justified.

Keywords: Kuhn-Tucker conditions; Third order shear deformation theory; Functionally graded porous beam.

1. Introduction

Microstructure affects material behavior. Materials engineers modify microstructure via processing. Traditional processing studies might optimize microstructural properties for uniformity. Same-microstructure improves characteristics. Functionally graded materials (FGMs) [1] are unique materials with varied microstructures and features that increase performance and dependability in a certain application or boundary conditions. Microstructure is a position-dependent variable [2], therefore it may mix materials in one section. FGMs are purpose-built microstructural materials systems. FGM interlayers steadily modify ceramic and metal proportions. Aerospace, marine, and civil engineers employ porous material [3], [4]. These compounds alter porousness steadily as you go through them. Porous foundation material has holes in various places. Pore size and number affect porosity [5].

Static and moving load responses of FGM structures are essential in structural design. Theories [6] anticipate FGM constructions' mechanical load responses. The two-layer shear deformation hypothesis of Nguyen et al. [7] explains beam bending. Wattanasakulpong [8] investigated porous beam linear and nonlinear vibration using classical beam theory (CBT). CBT only works for thin beams because it ignores shear deformation. The First Order Beam Theory

* Corresponding author: E-mail address: nkgeeth@gmail.com

(FBT) [9] accounts for shear deformation in medium-thick beams because of its importance. Chen et al. [10] analyzed porous beams for static, buckling, and vibration [11]. Wu et al. [12] examined beam structural dynamics. Gao et al. [13] used FBT to calculate beam frequencies computationally. Noori et al. [14] examined beam frequency changes. They used FBT and complementing functionalities. Lei et al. [15] studied FG beam dynamics. Magnucka [16] modified Timoshenko beam theory (TBT) to analyze sandwiched beams for dynamic and static stability.

Higher-order beam theories (HBT) [17, 18] may solve FGP beam problems. Wattanasakulpong et al. [19] calculated porous beam free vibrations using third-order beam theory and Chebyshev collocation. Beams placed on foundations were analyzed using the novel polynomial [20], trigonometric [21], and exponential shear functions [22]. Polit et al. [23] created an HBT to calculate curved beam stability and bending. HBTs don't need shear correction factors since they employ shear shape functions. Shear shape functions affect HBT accuracy. Researchers created more than shear shape functions. They revised theories to reduce unknowns. Shimpi [24] divided displacement fields into shear and bending components to better analyze isotropic plates. Akbaş [25] offered FEM for beam stability and natural frequencies analysis. Anirudh et al. [26] employed a FEM to analyze variations in a curved beam. Fang et al. [27] used iso-geometric analysis for static and vibration analysis. Ebrahimi [28] employed the differential transform approach to analyze rotating beam vibration, whereas [29] used the Transfer Matrix Method to study porous beam vibration. Zhao et al. [30] studied deep-curved beam vibration using modified Fourier series. Jamshidi [31] used the Ritz approach to investigate how FG beams vibrate and fail to design them.

Earlier studies have mostly examined the bending characteristics of bi-directional functionally graded porous beams. The novelty of the present study incites a mathematical approach in adapting the Kuhn-Tucker (KT) conditions solution approach and R-program to assess the significance of the elastostatic behavior of a two directional functionally graded porous beams (FGPB) and solve equilibrium equations under specified boundary conditions and material distributions.

This is apparent based on the utilization of deformation theories in the aforementioned debates. The significance of thickness is crucial, especially in the context of two-dimensional functionally graded porous beams. Therefore, it is essential to investigate the shear and normal deformation theory in conjunction with different boundary conditions, aspect ratios, and gradation exponents. The utilization of the higher order shear deformation theory (HSDT) has been found to yield precise outcomes in the field of structural analysis. Therefore, the HSDT with a third-order accuracy is employed to analyze the bending characteristics of a FGPB under prescribed boundary conditions adapting KT conditions with R- program. Numerical calculations are conducted to ascertain the maximum transverse deflections, axial stresses, transverse shear stresses, and normal stresses for different gradation exponents, aspect ratios (L/h), and porosity levels (both even and uneven) in simply-supported (SS) and clamped-clamped (CC) beams.

2. Nomenclature

2D-FGB	Two directional functionally graded beam
CBT	Classical beam theory
CC	Clamped clamped
FBT	First order beam theory
FGM	Functionally graded materials
FGPB	Two directional functionally graded porous beam
HBT	Higher order beam theory
HSDT	Higher order shear deformation theory
SS	Simply supported
TBT	Timoshenko beam theory
UDL	Uniformly distributed load

3. Formulation and mathematics

3.1. Formulation of functionally graded porous beam

In the light of HSDT, a beam is modelled as a slender structural element exhibiting bending and shear behaviour. The beam is assumed to be straight and uniform along its length, with small deformations and linearized equations. Warping effects, involving twisting of the cross-section, are disregarded, and the assumption is made that the initially plane cross-sections remain plane after deformation. Material properties are considered to be constant throughout the beam, simplifying calculations and analytical solutions. The coordinate system utilized for FGPB in the current study is depicted in Figure 1. The material properties exhibit continuous variation along the length and thickness directions. A FGPB is modelled through the gradation of ceramic and metallic phases along the direction of thickness. The bottom

portion of beam located at z = -h/2 is composed of ceramic, while the upper portion at z = +h/2 is comprised of metal. The volume percentage of the component materials determines the material characteristics of FGPB.

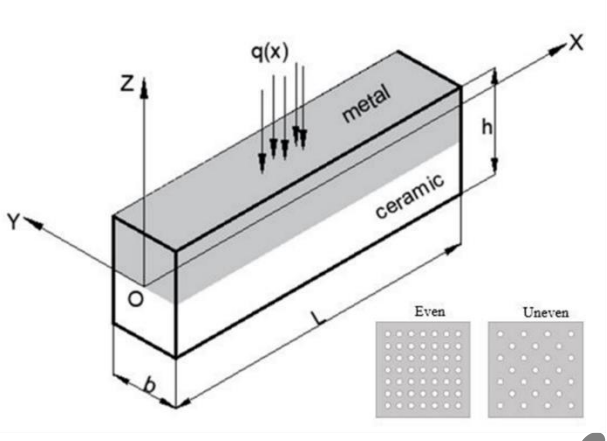

Fig 1: Beam that is functionally graded, with even and uneven porosity

It is to be anticipated that there will be a relationship, both functional and structural, among the thickness and the material's properties. As demonstrated in Eq. 1, the power law distribution in *x* and *z* could be utilized to accurately express the volume fraction of one constituent as (V_{f1}) [32].

$$V_f(x,z) = \left(\frac{z}{h}+\frac{1}{2}\right)^{P_z}\left(\frac{x}{L}+\frac{1}{2}\right)^{P_x} \tag{1a}$$

$$\mathrm{V_{f1}(x,z) + V_{f2}(x,z) = 1} \tag{1b}$$

In this context, P_x and P_z are the gradient indices which describe the volume fraction over the whole course of the length as well as the thickness of the beam, respectively. It is then possible to express the functional characteristics of the material (P) of evenly distributed FGPB as [33],

$$P(x,z) = (P_c - P_m)\left(\frac{z}{h}+\frac{1}{2}\right)^{P_z}\left(\frac{x}{L}+\frac{1}{2}\right)^{P_x} + P_m - \frac{\alpha}{2}(P_c + P_m) \tag{2a}$$

where α denotes the porosity coefficient ($0 \le \alpha \le 1$), m represents the presence of metal, whereas c denotes the presence of ceramic. As per the previously mentioned correlation, the Modulus of Elasticity (E) is utilized for the evaluation of material rigidity as well as the moment of inertia in an evenly distributed FGPB, and can be mathematically represented as stated in Eq. (2b).

$$E(x,z) = (E_c - E_m)\left(\frac{x}{L}+\frac{1}{2}\right)^{P_x}\left(\frac{z}{h}+\frac{1}{2}\right)^{P_z} + E_m - \frac{\alpha}{2}(E_c + E_m) \tag{2b}$$

Although there is a marginal variation when using Poisson's ratio contrasted to various properties, this is deemed to be unchanged as calculations are carried out employing the mean value. Similarly, one may determine the effective characteristics of the component with distributed but even FGPB using the Eq. (2c).

$$P(x,z) = (P_c - P_m)\left(\frac{z}{h}+\frac{1}{2}\right)^{P_z}\left(\frac{x}{L}+\frac{1}{2}\right)^{P_x} + P_m - \frac{\alpha}{2}(P_c + P_m)\left(1 - \frac{2|z|}{h}\right) \tag{2c}$$

E for unevenly distributed FGPB could be approximated through the use of Eq. (2d).

$$E(x,z) = (E_c - E_m)\left(\frac{z}{h}+\frac{1}{2}\right)^{P_z}\left(\frac{x}{L}+\frac{1}{2}\right)^{P_x} + E_m - \frac{\alpha}{2}(E_c + E_m)\left(1 - \frac{2|z|}{h}\right) \tag{2d}$$

Static and dynamic structures require well-designed FG beams and plates. This reduces production costs. The buckling, bending, and vibration evaluation of FGM structures designed using traditional beam and plate theories usually overestimates structural deflections, critical loads, critical buckling and natural frequencies. Standard beam and plate theories determine critical loads and natural frequencies. Thus, shear deformation FG beam theories should be used to increase forecast accuracy. The Cartesian coordinate system of the FGPB starts at the neutral beam axis while the beam's thickness limits the deformations and extension, bending, buckling and shear cause *x*-direction displacements. Porosity affects the transverse shear as well as the normal strain. The displacement field that satisfies the postulates of the beam are based on the constitutive equations, Eqs. (3a), and (3b) [33, 34].

$$U(x,z) = u_0(x) + z\emptyset(x) - f(z)\left(\emptyset(x) + \frac{\partial w_0}{\partial x}(x)\right) \quad (3a)$$

$$W(x,z) = w_0(x) \quad (3b)$$

where axial as well as transverse displacements are represented by U and W respectively. At any given position along the neutral axis, u_0 and w_0 represent the axial as well as transverse displacements, respectively. The bending slope is denoted by $\frac{\partial w_0}{\partial x}$, and $\emptyset$ the shear slope. The transverse shear deformation may be determined by utilizing the shape function $f(z)$, and the mathematical equations describing the non-zero strains could be obtained by using Eqs. (4a) and (4b), respectively, as,

$$\varepsilon_x = \frac{\partial U}{\partial x} = \frac{\partial u_0}{\partial x} - z\frac{\partial^2 w_0}{\partial x^2} + f(z)\left(\frac{\partial \emptyset}{\partial x} + \frac{\partial^2 w_0}{\partial x^2}\right) \quad (4a)$$

$$W(x,z) = w_0(x) \quad (3b)$$

where axial as well as transverse displacements are represented by U and W respectively. At any given position along the neutral axis, u_0 and w_0 represent the axial as well as transverse displacements, respectively. The bending slope is denoted by $\frac{\partial w_0}{\partial x}$, and $\emptyset$ the shear slope. The transverse shear deformation may be determined by utilizing the shape function $f(z)$ [34], and the mathematical equations describing the non-zero strains could be obtained by using Eqs. (4a) and (4b), respectively, as,

$$\varepsilon_x = \frac{\partial U}{\partial x} = \frac{\partial u_0}{\partial x} - z\frac{\partial^2 w_0}{\partial x^2} + f(z)\left(\frac{\partial \emptyset}{\partial x} + \frac{\partial^2 w_0}{\partial x^2}\right) \quad (4a)$$

$$\gamma_{xz} = f'\left[\emptyset(x) + \frac{\partial w_0}{\partial x}\right] \quad (4b)$$

$$f(z) = \frac{4z^3}{3h^2} \quad (5)$$

In accordance with Hooke's Law and with the assistance of Eqs. (4a), and (4b), the following field equations representing stress could be derived:

$$\sigma_x = E(x)\varepsilon_x \quad (6a)$$

$$\tau_{xz} = \frac{E(x)}{2(1+\mu)}\gamma_{xz} \quad (6b)$$

3.2. Governing equations

The governing equations can be deduced by beginning with the principle of virtual displacements. The principle that actual work can be performed result in,

$$\int_0^t (\delta U + \delta V)\, dt = 0 \quad (7)$$

where, t is time, δU, δV, are variations in strain energy, and variation of work done, respectively. Variation in strain energy in a FGPB is shown in Eq. (8).

$$\delta U = \frac{1}{2}\int_0^L \int_{-\frac{h}{2}}^{+\frac{h}{2}} (\sigma_x \varepsilon_x + \tau_{xz}\gamma_{xz}) dz dx \tag{8}$$

$$\delta V = -\int_0^L q\delta w_0 \, dx \tag{9}$$

The beam's bending stress in regards of virtual strain energy as work energy can be demonstrated by,

$$B = \delta U + \delta V = 0 \tag{10}$$

$$\int_0^L \int_{-\frac{h}{2}}^{\frac{h}{2}} (\sigma_x \delta\varepsilon_x + \tau_{xz}\delta\gamma_{xz}) dz dx - \int_0^L q\delta w_0 \, dx = 0 \tag{11}$$

$$\int_0^L \int_{-h/2}^{h/2} \left(\sigma_x \delta\left(\frac{\partial u_0}{\partial x} - z\frac{\partial^2 w_0}{\partial x^2} + f(z)\left(\frac{\partial \phi}{\partial x} + \frac{\partial^2 w_0}{\partial x^2}\right)\right) + \tau_{xz\delta} f'(z)\left[\emptyset + \frac{\partial w_0}{\partial x}\right]\right) dz dx - \int_0^L q\delta w_0 \, dx = 0 \tag{12}$$

$$\int_0^L \left(\frac{\partial N_x \delta u_0}{\partial x} - \frac{\partial^2 M_b \delta w_0}{\partial x^2} + \frac{\partial M_s \delta\emptyset}{\partial x} + \frac{\partial^2 M_s \delta w_0}{\partial x^2} + Q_{xz}\delta\emptyset + \frac{\partial Q_{xz}\delta w_0}{\partial x}\right) dx - \int_0^L q\delta w_0 \, dx = 0 \tag{13}$$

$$\begin{bmatrix} N_x \\ M_b \\ M_s \end{bmatrix} = \int_{-\frac{h}{2}}^{\frac{h}{2}} \sigma_x \begin{Bmatrix} 1 \\ z \\ f(z) \end{Bmatrix} dz \tag{14}$$

$$Q_{xz} = \int_{-\frac{h}{2}}^{\frac{h}{2}} \tau_{xz} f'(z) dz \tag{15}$$

$$\delta u_0 = \frac{\partial}{\partial x} N_x = 0 \tag{16a}$$

$$\delta w_0 = \frac{\partial^2}{\partial x^2} M_b - \frac{\partial^2}{\partial x^2} M_x + q - \frac{\partial}{\partial x} Q_{xz} = 0 \tag{16b}$$

$$\delta\emptyset = \frac{\partial}{\partial x} M_s + Q_{xz} = 0 \tag{16c}$$

3.3. Kuhn – Tucker conditions

Assume that $f_k(x)$ $(k = 0, 1, 2, \ldots\ldots m)$ are all differentiable if the function $f_0(x)$ attains at point x^0 a local minimum subject to the set $K = \left\{\frac{x}{f_i(x)} \leq 0 (i = 1, 2, 3, \ldots\ldots m)\right\}$ then there exist a vector of Lagrange multiplier U^0 such that the following conditions are satisfied.

$$\frac{\partial f_0(x^0)}{\partial x_j} + \sum_{i=1}^{m} U_i^0 \frac{\partial f_0(x^0)}{\partial x_j} = 0 \ (j = 1, 2, 3, \ldots\ldots, n)$$

$$f_i(x^0) \leq 0 \ (i = 1, 2, 3, \ldots. m)$$

$$u_i^0 f_i(x^0) = 0 \ (i = 1, 2, 3, \ldots., m)$$

$$u_i^0 \geq 0 \ (i = 1, 2, 3, \ldots. m)$$

These conditions are necessary conditions for a local minimum of problems, for maximization problems, the non-negativity condition $U^0 \leq 0$, are called the KT condition.

$$L(x, y, u) = f_0(x) + \sum_{i=1}^{m} u_i (f_i(x) + y_i^2)$$

The necessary condition for its local minimum are,

$$\frac{\partial L}{\partial x_j} = \frac{\partial f_0(x^0)}{\partial x_j} + \sum_{i=1}^{m} u_i^0 \frac{\partial [f_i(x^0) + (y_i^0)^2]}{\partial x_j} = 0$$

$$\frac{\partial L}{\partial y_i} = 2u_i^0 y_i^0 = 0 \ \ (j = 1, 2, 3, \ldots . n)$$

$$\frac{\partial L}{\partial u_i} = f_i(x^0) + (y_i^0)^2 = 0 \ \ (i = 1, 2, 3, \ldots m)$$

$$\frac{\partial f_0[x^0(b)]}{\partial b_i} = -u_i^0 \ \ (i = 1, 2, 3, \ldots . m)$$

Without slack variables, the mathematical problem,

$$L(x, u) = f_0(x) + \sum_{i=1}^{m} u_i f_i(x)$$

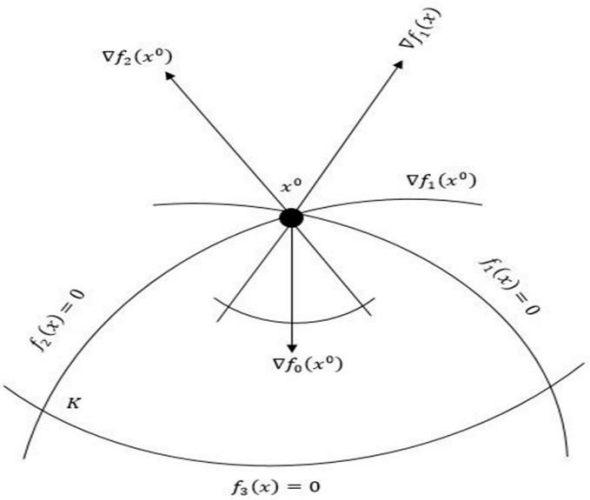

Fig 2: Kuhn Tucker condition

The KT condition can be rewritten as,

$$\frac{\partial L(x^0, u^0)}{\partial x_j} = 0 \ (j = 1, 2, 3, \ldots . n)$$

$$\frac{\partial L(x^0, u^0)}{\partial u_i} \leq 0 \ (i = 1, 2, 3, \ldots . m)$$

$$u_i^0 \ \frac{\partial L(x^0, u^0)}{\partial u_i} = 0 \ (i = 1, 2, 3, \ldots . m)$$

$$u_i^0 \geq 0 \ (i = 1, 2, 3, \ldots m)$$

If the multiplier u_i is positive, then the corresponding i[th] constraint is binding (boundary solution). When the function $u_0(x, y)$, $w_0(x, y)$, and $\emptyset_0(x, y)$ are expressed as generalized co-ordinates, it can be represented as Lagrange equations. KT condition can be written as follows:

$$u_0(x, y) = \sum_{i=1}^{m} f_i(x^0)\theta_i e^{i\lambda y} \quad (17)$$

$$w_0(x, y) = \sum_{i=1}^{m} f_i(x^0)\varphi_i e^{i\lambda y} \quad (18)$$

$$\emptyset_0(x, y) = \sum_{i=1}^{m} f_i(x^0)\psi_i e^{i\lambda y} \quad (19)$$

where, θ_i, φ_i, and ψ_i are the three different boundary conditions and λ is the scalar.

3.4. R-programming for KT conditions

R-programming in KT conditions can greatly enhance the efficiency and versatility of solving constrained optimization problems. KT conditions are a set of necessary conditions for the solution of nonlinear optimization problems with constraints. By integrating R programming into the analysis of KT conditions, one can take advantage of R's robust mathematical libraries and data manipulation capabilities. Incorporating R-program into the process allows for the efficient computation of gradients, Hessians, and constraint functions, which are crucial components of KT conditions. R's extensive package ecosystem, including 'optim', 'nloptr', and 'quadprog', can be leveraged to find numerical solutions to optimization problems while adhering to KT conditions. Furthermore, R's data visualization capabilities enable the effective representation of optimization results, aiding in the interpretation and decision-making process. By writing R scripts to handle KT conditions, practitioners gain a flexible and customizable approach to solving complex optimization problems with constraints. This integration not only streamlines the analysis but also provides a platform for rigorous sensitivity analysis and model validation, ensuring the reliability and accuracy of optimization solutions in various real-world applications. The inclusion of R-programming in KT conditions opens up a powerful avenue for tackling constrained optimization challenges efficiently and effectively.

```
for (i in 1:n)
  {
   A.mat[i,i]   <- 1        # coefficint for l_{t-1}
   A.mat[i,i+1] <- -1       # coefficint for l_[1]
   A.mat[i,n + 1 + i] <- 1   # coefficint for q_[1]
  }
  for(i in (n+1):(2*n))
  {
   A.mat[i,i+1] <- 1
   A.mat[i,n + 1 + i] <- - Kuhn-Tucker
  }
   A.mat[nrow(A.mat)-1,1] <- 1    # coefficint for i_[1]
   A.mat[nrow(A.mat),n+1] <- 1    # coefficint for i_[1]
   A.mat
   sol <- Rglpk_solve_LP(obj = c.vec, mat = A.mat, dir = const.vec, rhs = b.vec, types = vtype.vec)
   list( l = sol$solution[1:(n+1)],         # inventory levels
         q = sol$solution[(n+2):(2*n+1)],   # order quantities
         y = tail(sol$solution, n),         # order indicators
         d = d.vec )                        # demand
```

R-programming for KT conditions is utilized for mathematical calculations, as stated in Table 1.

Table 1. The boundary conditions based on the R- programming adapting KT conditions

Demand	$x = 0$	$x = L$
SS = q	$u = 0, w = 0$	$w = 0$
CC = y	$u = 0, w = 0, \emptyset = 0, w' = 0$	$u = 0, w = 0, \emptyset = 0, w' = 0$
CF = d	$u = 0, w = 0, \emptyset = 0, w' = 0$	--

From Table 1, the following conditions are framed:

$$\frac{\partial^2\pi}{\partial M_j^2} = 0, \frac{\partial^2\pi}{\partial N_j^2} = 0, \frac{\partial^2\pi}{\partial P_j^2} = 0 \tag{20}$$

$$\left\{\begin{bmatrix} F_{11} & F_{12} & F_{13} \\ F_{21} & F_{22} & F_{23} \\ F_{31} & F_{32} & F_{33} \end{bmatrix} - \lambda^2 \begin{bmatrix} 0 & 0 & 0 \\ 0 & R_{22} & 0 \\ 0 & 0 & 0 \end{bmatrix}\right\} \begin{bmatrix} M \\ N \\ P \end{bmatrix} = \begin{bmatrix} 0 \\ 0 \\ 0 \end{bmatrix}$$

$$\left\{\begin{bmatrix} F_{11} & F_{12} & F_{13} \\ F_{21} & F_{22} & F_{23} \\ F_{31} & F_{32} & F_{33} \end{bmatrix} - \begin{bmatrix} 0 & 0 & 0 \\ 0 & \lambda^2 R_{22} & 0 \\ 0 & 0 & 0 \end{bmatrix}\right\} \begin{bmatrix} M \\ N \\ P \end{bmatrix} = \begin{bmatrix} 0 \\ 0 \\ 0 \end{bmatrix}$$

$$F_{11}(i,j) = M \int_0^L e^{\lambda x(x+1)}\, \theta_{i,x}, \theta_{j,x} dx$$

$$F_{12}(i,j) = F_{21}(i,j) = P \int_0^L e^{\lambda x(x+1)}\, \theta_{i,x}, \theta_{j,x} dx$$

$$F_{13}(i,j) = F_{31}(i,j) = (N - \alpha M) \int_0^L e^{\lambda(x+1)}\, \theta_{i,x}, \varphi_{i,x} dx$$

$$F_{22}(i,j) = \alpha^2 [F_{12}(i,j)][F_{13}(i,j)]$$

$$F_{23}(i,j) = F_{32}(i,j) = (\beta^2 - \alpha F)[F_{22}(i,j)]$$

$$F_{33}(i,j) = \lambda^2 R_{22} \int_0^L e^{\lambda x(x+1)}\, \theta_i, \theta_i dx$$

$$R_{11} = R_{12} = R_{13} = R_{21} = R_{23} = R_{31} = R_{32} = R_{33} = 0$$

$$R_{22}(i,j) = (\alpha^2 M - \beta N)[F_{33}(i,j)]$$

where, $i, j = 1, 2, 3, \ldots\ldots n$

4. Numerical computation and discussion

The proposed methodology can be assessed by employing a specific case study. This analysis encompasses the influence of gradient indexes, aspect ratio, and porosity index, specifically the composition of materials, on the bending characteristics of FGPB. The physical properties of the material [35] of the FGPB in the current study are as follows:

Alumina: E_c = 380 GPa, μ_c = 0.3

Aluminium: E_m= 70 GPa, μ_m = 0.3

Non-dimensional maximum transverse deflection ($\overline{w}$) for SS and CC beams could be estimated using Eq. (21) and Eq. (22) for CF beam.

$$\overline{w} = \frac{100 E_m h^3}{q_0 L} w(x, 0) \tag{21a}$$

$$\overline{w} = \frac{100 E_m h^3}{q_0 L} w(L, 0) \tag{21b}$$

The axial stress ($\overline{\sigma}_x$) could be estimated using Eq. (23).

$$\overline{\sigma}_x = \frac{\sigma_x h}{q_0 L} \tag{22}$$

The transverse shear stress ($\overline{\tau}_{xz}$) could be estimated using Eq. (23).

$$\overline{\tau}_{xz} = \frac{\tau_{xz} h}{q_0 L} \tag{23}$$

The normal shear stress ($\overline{\sigma}_{xz}$) could be estimated using Eq. (24).

$$\overline{\sigma}_{xz} = \frac{\sigma_{xz} h}{q_0 L} \tag{24}$$

Numerical results may be obtained using various gradation exponents in both directions (*x* and z), aspect ratios, and boundary conditions. A uniformly distributed load (UDL) is imparted to test the FGPB and the obtained results on transverse deflection, axial stress, shear stress, and normal stress are compared with earlier investigations [36, 37] and presented in Table 2.

Table 2. Validation of HSDT with SS boundary condition

Function	Method	P = 0	P = 1	P = 2	P = 5	P = 10
Transverse deflection	L/h = 5					
	[36]	3.1654	6.2594	8.0677	9.8281	10.9381
	[37]	3.1654	6.259	8.0668	9.8271	10.9375
	Present	3.1539	6.3171	8.123	9.6832	10.7834
	L/h = 20					
	[36]	2.8962	5.8049	7.4421	8.8182	9.6905
	[37]	2.8963	5.8045	7.4412	8.8173	9.6899
	Present	2.9231	5.8123	7.5347	8.8233	9.6231
Axial stress	L/h=5					
	[36]	3.802	5.8836	6.8826	8.1106	9.7122
	[37]	3.804	5.887	6.886	8.115	9.717
	Present	3.8122	5.7882	6.7822	8.2112	9.7102
	L/h=20					
	[36]	15.0129	23.2053	27.0991	31.813	38.1385
	[37]	15.02	23.22	27.11	31.83	38.16
	Present	15.0132	23.1832	27.1023	31.7812	38.1251
Transverse shear stress	L/h=5					
	[36]	0.7332	0.7332	0.6706	0.5905	0.6467
	[37]	0.7335	0.7335	0.67	0.5907	0.6477
	Present	0.7324	0.7423	0.7021	0.6109	0.6322
	L/h=20					
	[36]	0.7451	0.7451	0.6824	0.6023	0.6596
	[37]	0.747	0.747	0.6777	0.6039	0.6682
	Present	0.7581	0.7442	0.6811	0.6102	0.6587
Normal shear stress	L/h=5					
	[36]	0.1352	0.0672	0.0927	0.0182	-0.0179
	[37]	0.1352	0.0671	0.0925	0.0182	-0.018

Present	0.1432	0.0702	0.0899	0.0201	-0.0212
L/h=20					
[36]	0.0338	-0.5874	-0.6261	-1.169	-1.556
[37]	0.0338	-0.588	-0.6226	-1.176	-1.5589
Present	0.0381	-0.5992	-0.6132	-1.2012	-1.4997

4.1. Transverse deflection of a FGPB as a function of porosity and gradient exponents

FGPB under UDL is analyzed at aspect ratio and gradation exponents to evaluate how porosity (even and uneven) affects transverse deflection. Aspect ratio reduces dimensionless transverse deflections. Uneven porosity in FGPB may modify stress distribution considerably as seen in Fig. 3.

As shown in Fig. 3, transverse deflections increases in two directions with increasing porosity index. Uneven porosity in the beam distributes voids unevenly which causes material stiffness to vary, causing various beam regions to deflect differently under load. Porosity affects deflection in which, the FGPB with even porosity might have a steeper material property gradient over its thickness with a greater gradation exponent. Stiffening the material reduces the transverse deflection under the same force while the volume proportion and size of the voids and the material qualities at the end of beam presents the effect of gradation exponent on transverse deflection [35]. Gradation exponent affects transverse deflection more complexly in SS beams with unequal porosity in which, at the places with significant porosity, a larger gradation exponent might enhance material property fluctuation and deflection [36]. A greater gradation exponent may also stiffen the material in low-porosity parts, offsetting the increased deflection in high-porosity regions. The gradation exponent's influence on transverse deflection in a beam with unequal porosity relies on its distribution and variance. Porosity effects the transverse deflection, wherein, the amount of bending perpendicular to the beam's length when a load is applied, in CC beams.

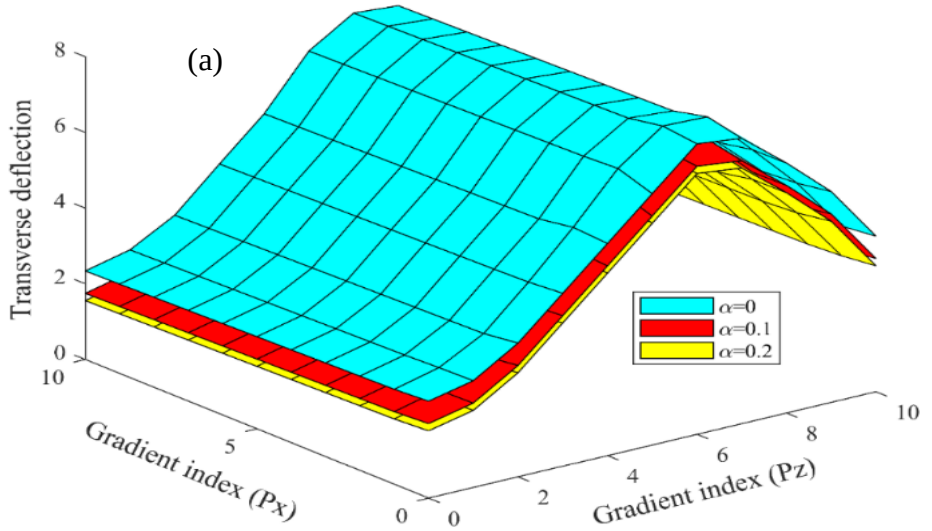

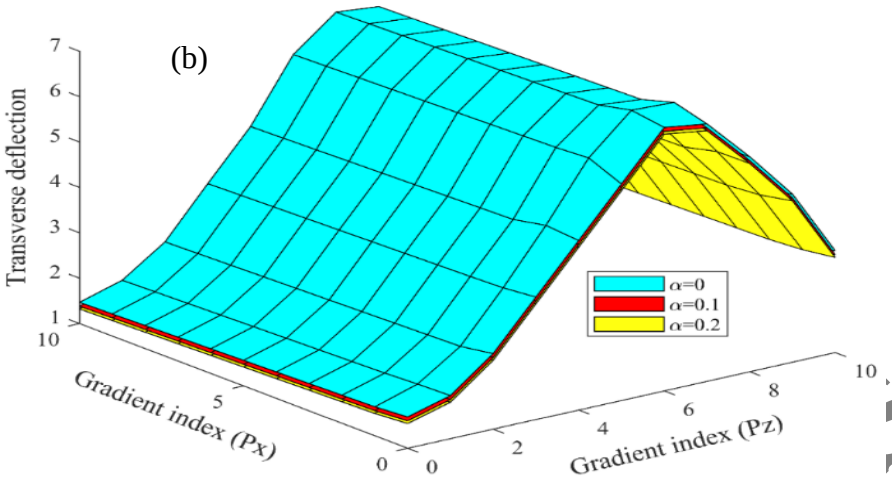

Fig 3: Comparison of transverse deflections of SS beam having (a) even and (b) uneven porosity, and gradient index

Fig. 4 illustrates that equal porosity in the beam distributes voids evenly which reduces the material stiffness. The CC boundary condition further requires a beam node positioned at the center. Voids reduces the uniformity of the material, hence reducing the beam's ability to support this specific location, resulting in an increase in deflection [35] [37]. A greater gradation exponent may increase material property gradients along the beam with even porosity. This may stiffen the material and minimize transverse deflection under stress. A steeper gradient of material qualities makes the beam's material more uniform, making it simpler to retain the CC boundary conditions' nodal point near the center.

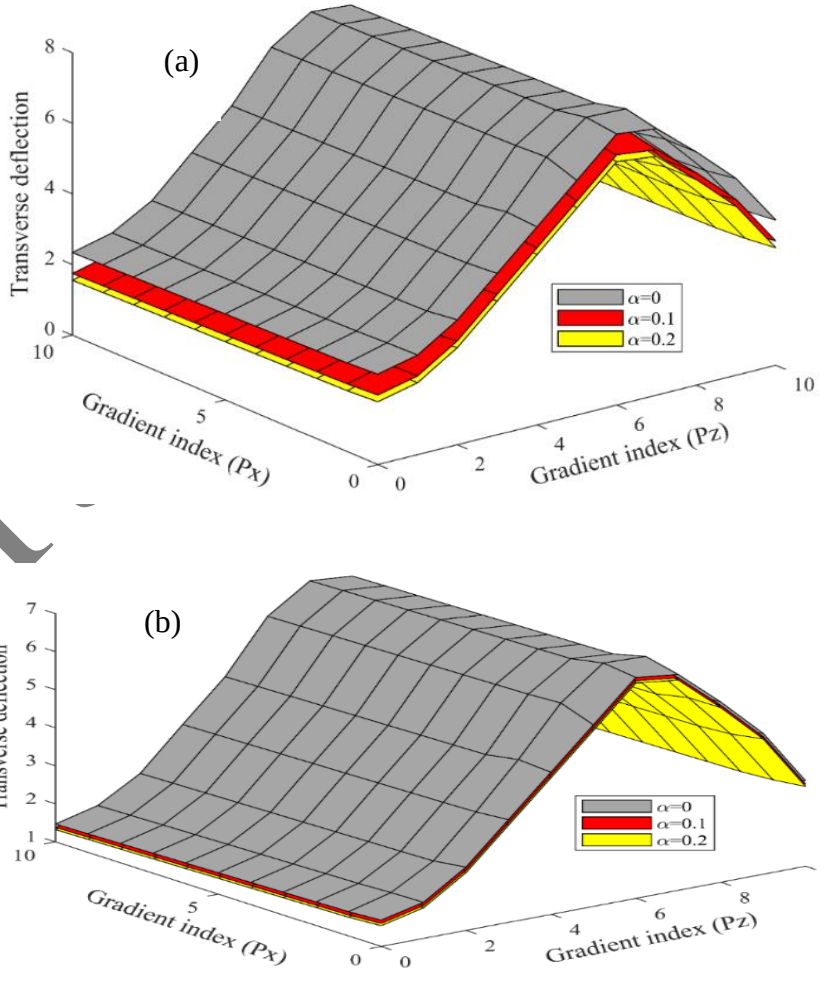

Fig 4: Comparison of transverse deflections of CC beam having (a) even and (b) uneven porosity, and gradient index

4.2. Axial stress of a FGPB as a function of porosity and gradient exponents

Porosity affects mechanical parameters like Young's modulus and Poisson's ratio in SS beams with even porosity. As can be seen from Fig. 5, more porosity may reduce stiffness and increase deformation under axial load, increasing beam axial stress. This may cause non-uniform beam deformation and stress distribution, with lower porosity parts having greater stress and higher porosity areas having lower stress. The gradient index affects axial stress based on material porosity and beam loading circumstances. A larger gradient index may provide a sharper material property gradient through the thickness of an SS beam with even porosity. This may make the material stiffer and less deformable under axial loading, lowering axial stress. Nevertheless, larger porosity may weaken the material and make it more deformable under axial loading, increasing axial stress. Gradient index affects axial stress differently in SS beams with unequal porosity. Porosity distribution may impact material characteristics throughout the beam's thickness, affecting its capacity to withstand deformation under axial stress. A steeper gradient of material characteristics in locations with reduced porosity might enhance stiffness and reduce axial loading deformation. Nevertheless, regions with larger porosity may be weaker and more prone to deformation under axial loading, increasing axial stress.

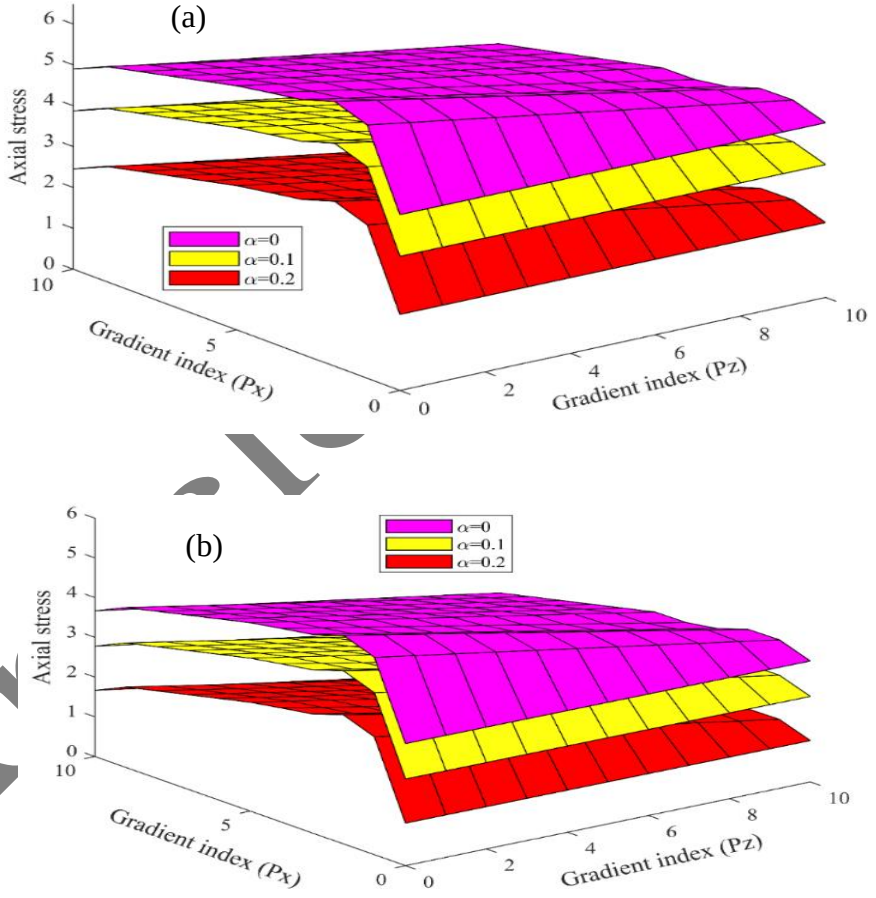

Fig 5: Comparison of axial stress of SS beam having (a) even and (b) uneven porosity, and gradient index

As demonstrated in Fig. 6, a CC beam with unequal porosity may vary in stiffness and deformation throughout its thickness. Low-porosity regions are stiffer and less deformable, lowering axial stress. Higher porosity weakens and deforms the material, increasing axial stress. Gradation exponents affect the material's characteristics over a CC beam's thickness, affecting axial stress. In a CC beam with uniform porosity, gradation exponents may affect material stiffness and deformation throughout the beam thickness. Stiffness and deformation vary more with a larger gradation exponent because material qualities change faster with thickness. This may balance out beam stresses, lowering axial stress.

Nevertheless, a smaller gradation exponent will result in a more gradual change in material characteristics throughout the beam thickness, which might cause uneven stress distribution and greater axial stress. Gradation exponents may complicate axial stress in CC beams with unequal porosity.

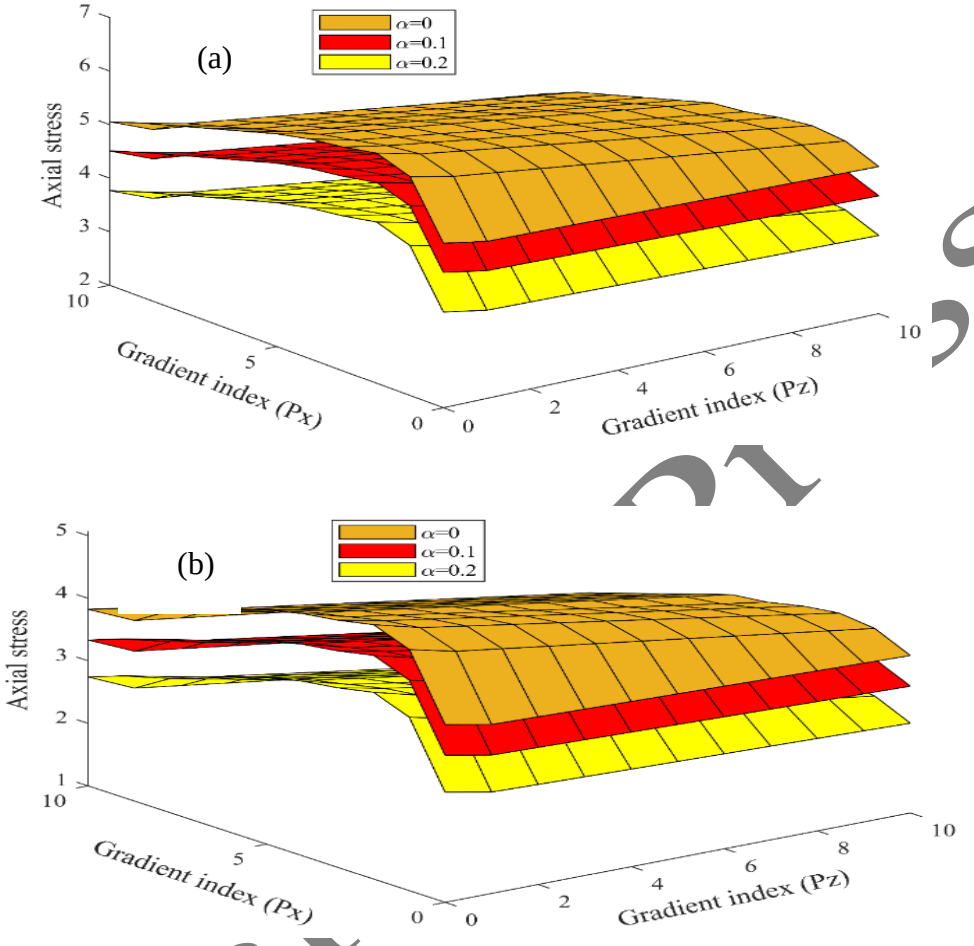

Fig 6: Comparison of axial stress of CC beam having (a) even and (b) uneven porosity, and gradient index

4.3. Shear stress of a FGPB as a function of porosity and gradient exponents

Fig. 7 shows SS beam porosity and gradient index effects. Shear stress will be generally consistent throughout the beam if porosity is even. Nevertheless, variable porosity will change shear stress. Shear stress is greatest in the least porous regions of a beam and lowest in the most porous. The least porous sections of the beam are stiffer and resist deformation better, resulting in larger shear stresses. The most porous portions of the beam will deform more and have lower shear stresses.

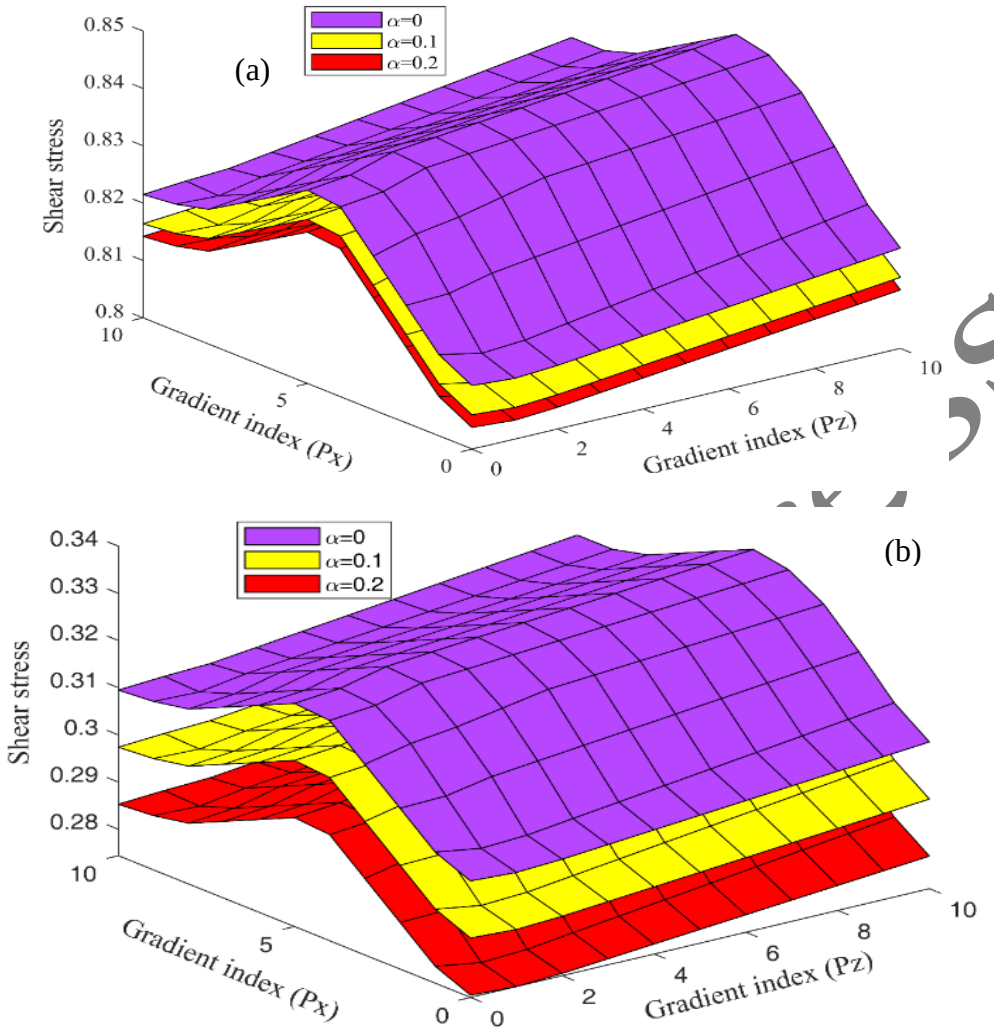

Fig 7: Comparison of shear stress of SS beam having (a) even and (b) uneven porosity, and gradient index

Fig. 8 shows CC beam porosity and gradient index effects. Shear stress is greatest near the middle of a CC beam and lowest at the clamped ends. Shear stress will be generally consistent throughout the beam if porosity is even. Shear stress will change if porosity varies along the beam. Shear stress is greatest in the least porous regions of a CC beam with variable porosity and lowest in the most porous. The least porous sections of the beam are stiffer and resist deformation better, resulting in larger shear stresses. The most porous portions of the beam will deform more and have lower shear stresses. Gradation exponents affect shear stress more in CC beams. A higher gradation exponent causes a greater difference in material characteristics along the beam, which may generate more deformation and shear stresses. The beam's lowest gradation exponent will have lower shear stresses. Porosity, gradation exponent, and material characteristics all impact shear stress. A greater gradation exponent, higher porosity, and lower stiffness might increase shear stress in the beam, particularly near the center. Bending moment also affects shear stress in CC beams. External weights or beam curvature create bending moments.

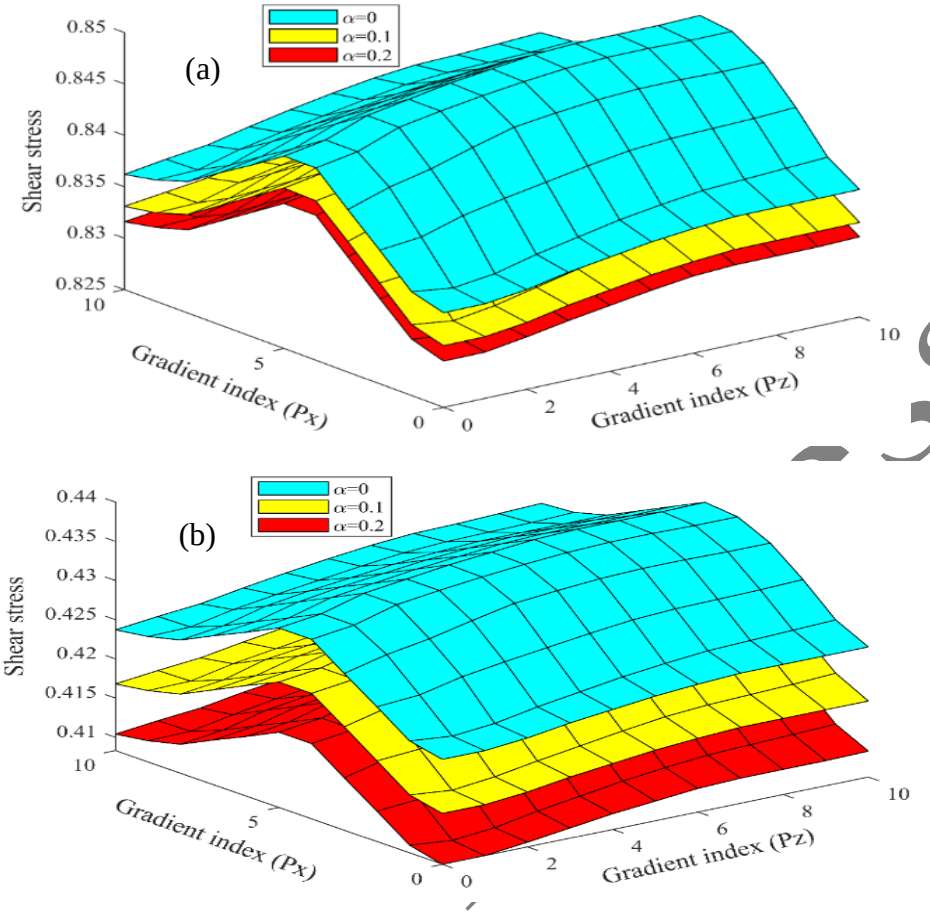

Fig 8: Comparison of shear stress of CC beam having (a) even and (b) uneven porosity, and gradient index

4.4. Normal stress of a FGPB as a function of porosity and gradient exponents

As demonstrated in Fig. 9, an SS beam with a greater gradation exponent changes material characteristics more quickly throughout its thickness. The bending moment, which depends on the applied load and material stiffness, determines SS beam normal stress. In a FGPB, material qualities may impact stiffness and normal stress. Higher gradation exponents increase beam normal stress, making the beam stiffer. A stiffer beam resists load deformation, increasing normal stress. Porosity complicates the influence of gradation exponent on normal stress. Void material reduces the effective cross-sectional area available to withstand deformation, decreasing beam stiffness. Increased porosity index lowers beam normal stress. The beam loses stiffness and deformability, lowering normal stress. Porosity lowers stiffness, while the surrounding material's greater stiffness compensates, resulting in a more complicated normal stress distribution.

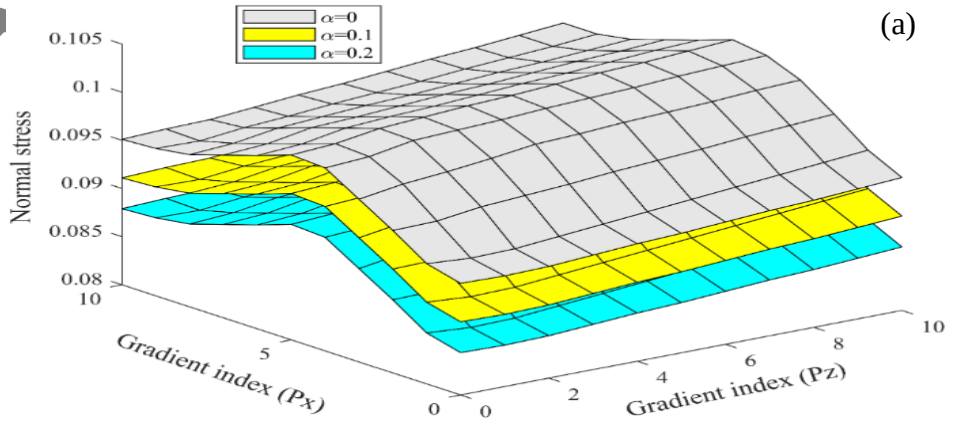

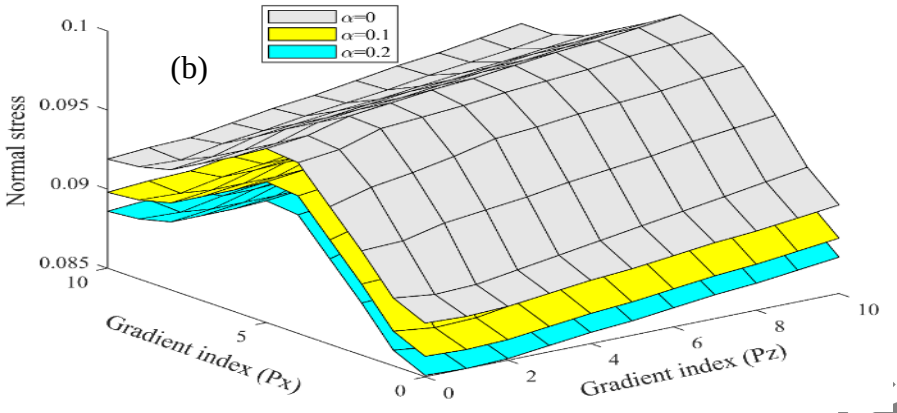

Fig 9: Comparison of normal stress of SS beam having (a) even and (b) uneven porosity, and gradient index

Fig. 10 shows the considerable influence of porosity on normal stress in a CC beam with uniform and uneven porosity. Higher porosity indexes reduce beam normal stress. Because material gaps or pores weaken the beam. A CC beam with unequal porosity may have sections with greater porosity index. Gradation exponents may significantly affect normal stress in CC beams with unequal porosity. Higher gradation exponents increase beam normal stress. Since a larger gradation exponent accelerates material property changes over the beam's thickness and length, stiffness and strength vary more.

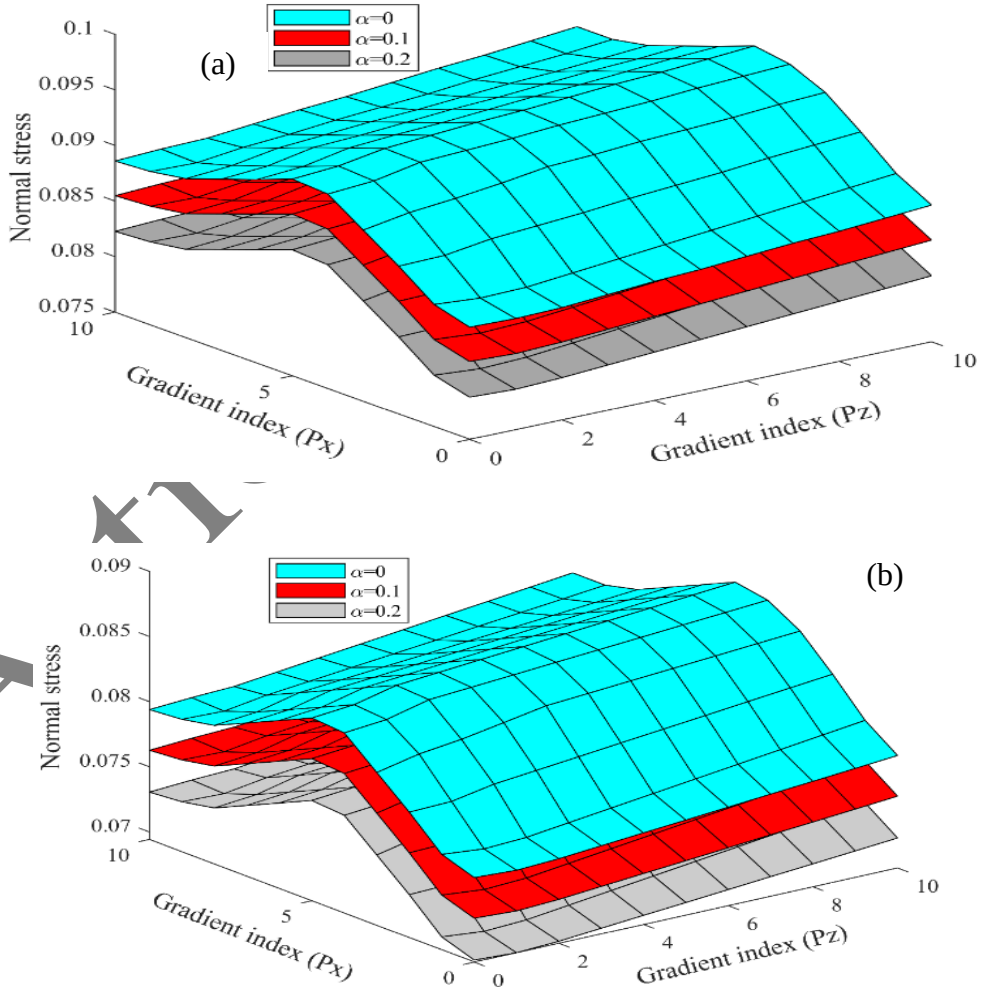

Fig 10: Comparison of normal stress of CC beam having (a) even and (b) uneven porosity, and gradient index

5. Conclusion

HSDT is utilized to conduct an analysis of the elastostatic behavior of FGPB that has been subjected to varied boundary conditions and a uniform load using a rigorous formulation. Transverse deflections, axial, shear, and normal stresses are estimated. The accuracy of the new approach is evaluated by analyzing a FGPB with simple support and the obtained results are compared with those of previous research. Consideration is given to three distinct border conditions: SS, CC, and CF. these conditions feature distinct gradation exponents in the length and thickness directions, as well as various aspect ratios. It has been determined that the HSDT method produces satisfactory outcomes. Noteworthy findings of the analysis are listed below:

- At $P_x = 0.1$ and $P_z = 0.1$, the transverse deflection for CF beam is found to be 20.007. While at $P_x = 0.5$ and $P_z = 0.5$, it is 15.512. Similarly for CC and SS beams, the transverse deflection at the same conditions were found to be 7.545, 3.807, 7.132, and 3.125. The CF beam typically exhibits the most significant effect, followed by the CC and SS beams.
- In a SS beam, increasing the gradient index results in a decrease in axial stress near the supports and an increase in axial stress at the center of the beam. In a CC beam, increasing the gradient index results in a decrease in axial stress at the center of the beam and an increase in axial stress near the clamped ends.
- Increasing the gradient index has a decreasing effect on the shear stress in a SS beam. In a CC beam, the effect of gradient index on shear stress is dependent on the distribution of the porosity. For even porosity, increasing the gradient index leads to a decrease in shear stress, while for uneven porosity, increasing the gradient index leads to an increase in shear stress.
- The effect of gradient index on normal stress is more pronounced in the middle region of SS, and CC beams, where the bending moment is maximum. In this region, a higher gradient index leads to a more uniform stress distribution and a lower stress concentration, which reduces the maximum normal stress in the beam.

Even or unequal porosity affects FGPB stress distribution. Even porosity decreases material strength and may generate stress concentrations in locations with greater porosity, although the impact on stress distribution is insignificant for typical stress. Uneven porosity, on the other hand, might cause stress concentrations in unexpected areas. Due to the averaging effect across a broader region, FGPB porosity has no influence on normal stress.

References

[1] Y. Miyamoto, W. Kaysser, B. Rabin, A. Kawasaki, R. G. Ford, Processing and fabrication, *Functionally Graded Materials: Design, Processing and Applications*, pp. 161-245, 1999.

[2] K. K. Chawla, K. K. Chawla, 1998, *Metal matrix composites*, Springer,

[3] J. Kim, K. K. Żur, J. Reddy, Bending, free vibration, and buckling of modified couples stress-based functionally graded porous micro-plates, *Composite Structures*, Vol. 209, pp. 879-888, 2019.

[4] J. Parthasarathy, B. Starly, S. Raman, A design for the additive manufacture of functionally graded porous structures with tailored mechanical properties for biomedical applications, *Journal of Manufacturing Processes*, Vol. 13, No. 2, pp. 160-170, 2011.

[5] K. Magnucki, P. Stasiewicz, Elastic buckling of a porous beam, *Journal of theoretical and applied mechanics*, Vol. 42, No. 4, pp. 859-868, 2004.

[6] M. Babaei, F. Kiarasi, K. Asemi, M. Hosseini, Functionally graded saturated porous structures: A review, *Journal of Computational Applied Mechanics*, Vol. 53, No. 2, pp. 297-308, 2022.

[7] N.-D. Nguyen, T.-N. Nguyen, T.-K. Nguyen, T. P. Vo, A new two-variable shear deformation theory for bending, free vibration and buckling analysis of functionally graded porous beams, *Composite Structures*, Vol. 282, pp. 115095, 2022.

[8] N. Wattanasakulpong, B. G. Prusty, D. W. Kelly, Thermal buckling and elastic vibration of third-order shear deformable functionally graded beams, *International Journal of Mechanical Sciences*, Vol. 53, No. 9, pp. 734-743, 2011.

[9] A. Melaibari, R. M. Abo-bakr, S. Mohamed, M. Eltaher, Static stability of higher order functionally graded beam under variable axial load, *Alexandria Engineering Journal*, Vol. 59, No. 3, pp. 1661-1675, 2020.

[10] D. Chen, S. Kitipornchai, J. Yang, Nonlinear free vibration of shear deformable sandwich beam with a functionally graded porous core, *Thin-Walled Structures*, Vol. 107, pp. 39-48, 2016.

[11] D. Chen, J. Yang, S. Kitipornchai, Free and forced vibrations of shear deformable functionally graded porous beams, *International journal of mechanical sciences*, Vol. 108, pp. 14-22, 2016.

[12] D. Wu, A. Liu, Y. Huang, Y. Huang, Y. Pi, W. Gao, Dynamic analysis of functionally graded porous structures through finite element analysis, *Engineering Structures*, Vol. 165, pp. 287-301, 2018.

[13] K. Gao, R. Li, J. Yang, Dynamic characteristics of functionally graded porous beams with interval material properties, *Engineering Structures*, Vol. 197, pp. 109441, 2019.

[14] A. R. Noori, T. A. Aslan, B. Temel, Dynamic analysis of functionally graded porous beams using complementary functions method in the Laplace domain, *Composite Structures*, Vol. 256, pp. 113094, 2021.

[15] Z. Lei, L. Zhang, K. Liew, J. Yu, Dynamic stability analysis of carbon nanotube-reinforced functionally graded cylindrical panels using the element-free kp-Ritz method, *Composite Structures*, Vol. 113, pp. 328-338, 2014.

[16] E. Magnucka-Blandzi, Mathematical modelling of a rectangular sandwich plate with a metal foam core, *Journal of theoretical and applied mechanics*, Vol. 49, No. 2, pp. 439-455, 2011.

[17] N. Hebbar, I. Hebbar, D. Ouinas, M. Bourada, Numerical modeling of bending, buckling, and vibration of functionally graded beams by using a higher-order shear deformation theory, *Frattura ed Integrità Strutturale*, Vol. 14, No. 52, pp. 230-246, 2020.

[18] L. Hao-nan, L. Cheng, S. Ji-ping, Y. Lin-quan, Vibration analysis of rotating functionally graded piezoelectric nanobeams based on the nonlocal elasticity theory, *Journal of Vibration Engineering & Technologies*, Vol. 9, pp. 1155-1173, 2021.

[19] P. Tossapanon, N. Wattanasakulpong, Flexural vibration analysis of functionally graded sandwich plates resting on elastic foundation with arbitrary boundary conditions: Chebyshev collocation technique, *Journal of Sandwich Structures & Materials*, Vol. 22, No. 2, pp. 156-189, 2020.

[20] M. Filippi, M. Petrolo, S. Valvano, E. Carrera, Analysis of laminated composites and sandwich structures by trigonometric, exponential and miscellaneous polynomials and a MITC9 plate element, *Composite Structures*, Vol. 150, pp. 103-114, 2016.

[21] X.-F. Li, B.-L. Wang, J.-C. Han, A higher-order theory for static and dynamic analyses of functionally graded beams, *Archive of Applied Mechanics*, Vol. 80, pp. 1197-1212, 2010.

[22] F. A. Fazzolari, Generalized exponential, polynomial and trigonometric theories for vibration and stability analysis of porous FG sandwich beams resting on elastic foundations, *Composites Part B: Engineering*, Vol. 136, pp. 254-271, 2018.

[23] O. Polit, C. Anant, B. Anirudh, M. Ganapathi, Functionally graded graphene reinforced porous nanocomposite curved beams: Bending and elastic stability using a higher-order model with thickness stretch effect, *Composites Part B: Engineering*, Vol. 166, pp. 310-327, 2019.

[24] R. Shimpi, P. Guruprasad, K. Pakhare, Simple two variable refined theory for shear deformable isotropic rectangular beams, *Journal of Applied and Computational Mechanics*, Vol. 6, No. 3, pp. 394-415, 2020.

[25] A. Assie, S. D. Akbas, A. M. Kabeel, A. A. Abdelrahman, M. A. Eltaher, Dynamic analysis of porous functionally graded layered deep beams with viscoelastic core, *Steel Compos. Struct*, Vol. 43, pp. 79-90, 2022.

[26] B. Anirudh, M. Ganapathi, C. Anant, O. Polit, A comprehensive analysis of porous graphene-reinforced curved beams by finite element approach using higher-order structural theory: Bending, vibration and buckling, *Composite Structures*, Vol. 222, pp. 110899, 2019.

[27] W. Fang, T. Yu, T. Q. Bui, Analysis of thick porous beams by a quasi-3D theory and isogeometric analysis, *Composite Structures*, Vol. 221, pp. 110890, 2019.

[28] F. Ebrahimi, N. Farazmandnia, Vibration analysis of functionally graded carbon nanotube-reinforced composite sandwich beams in thermal environment, *Advances in aircraft and spacecraft science*, Vol. 5, No. 1, pp. 107, 2018.

[29] Y. S. Al Rjoub, A. G. Hamad, Free Vibration of Axially Loaded Multi-Cracked Beams Using the Transfer Matrix Method, *International Journal of Acoustics & Vibration*, Vol. 24, No. 1, 2019.

[30] J. Zhao, Q. Wang, X. Deng, K. Choe, R. Zhong, C. Shuai, Free vibrations of functionally graded porous rectangular plate with uniform elastic boundary conditions, *Composites Part B: Engineering*, Vol. 168, pp. 106-120, 2019.

[31] M. Jamshidi, J. Arghavani, Optimal material tailoring of functionally graded porous beams for buckling and free vibration behaviors, *Mechanics Research Communications*, Vol. 88, pp. 19-24, 2018.

[32] P. Bridjesh, N. K. Geetha, G. Reddy, On Numerical Investigation of Buckling in Two-Directional Porous Functionally Graded Beam Using Higher Order Shear Deformation Theory, *Mechanics Of Advanced Composite Structures*, Vol. 10, No. 2, pp. 393-406, 2023.

[33] P. Bridjesh, N. Geetha, R. Ch, S. Nagaraju, ON NUMERICAL BUCKLING ANALYSIS OF TWODIRECTIONAL POROUS FUNCTIONALLY GRADED BEAM USING HIGHER ORDER SHEAR DEFORMATION THEORY, *Academic Journal of Manufacturing Engineering*, Vol. 21, No. 1, 2023.

[34] A. Karamanlı, Analytical solutions for buckling behavior of two directional functionally graded beams using a third order shear deformable beam theory, *Academic Platform-Journal of Engineering and Science*, Vol. 6, No. 2, pp. 164-178, 2018.

[35] T. P. Vo, H.-T. Thai, T.-K. Nguyen, F. Inam, J. Lee, Static behaviour of functionally graded sandwich beams using a quasi-3D theory, *Composites Part B: Engineering*, Vol. 68, pp. 59-74, 2015.

[36] A. Karamanlı, Bending analysis of two directional functionally graded beams using a four-unknown shear and normal deformation theory, *Politeknik Dergisi*, Vol. 21, No. 4, pp. 861-874, 2018.

[37] J. Reddy, C. Liu, A higher-order shear deformation theory of laminated elastic shells, *International journal of engineering science*, Vol. 23, No. 3, pp. 319-330, 1985.